Fission hindrance studies in ^{200}Pb: Evaporation residue cross section and spin distribution measurements

P. D. Shidling* and N. M. Badiger
Department of Physics, Karnatak University, Dharwad-580003, India

S. Nath, R. Kumar, A. Jhingan, R. P. Singh, P. Sugathan, S. Muralithar, and N. Madhavan
Inter University Accelerator Centre, New Delhi-110067, India

A. K. Sinha
UGC-DAE Consortium for Scientific Research, Kolkata Centre, Kolkata-700098, India

Santanu Pal
Variable Energy Cyclotron Centre, Kolkata-700064, India

S. Kailas
Nuclear Physics Division, Bhabha Atomic Research Centre, Mumbai-400085, India

S. Verma, K. Kalita, S. Mandal, and R. Singh
Department of Physics and Astrophysics, Delhi University, Delhi-110007, India

B. R. Behera
Department of Physics, Panjab University, Chandigarh-160014, India

K. M. Varier
Department of Physics, Calicut University, Calicut-673635, India

M. C. Radhakrishna
Department of Physics, Bangalore University, Bangalore-560056, India

(Received 26 September 2006; revised manuscript received 26 October 2006; published 7 December 2006)

Evaporation residue cross sections and spin distributions have been measured for ^{200}Pb compound nucleus formed in ^{16}O+^{184}W reaction at the laboratory beam energies of 84, 92, 100, 108, 116, and 120 MeV. The evaporation residues have been selected using the recoil mass spectrometer, HIRA and detected using a 2D position sensitive silicon detector. The evaporation residue spin distributions have been measured by detecting gamma rays with 14 element BGO multiplicity filter. Measured evaporation residue cross sections and spin distributions are compared with the values predicted by a standard statistical model code. Comparison shows that, in the energy region studied, the nuclear viscosity parameter $\gamma = 3$ is required to explain total evaporation residue cross sections and evaporation residue spin distributions.

DOI: 10.1103/PhysRevC.74.064603 PACS number(s): 25.70.Jj, 27.80.+w

I. INTRODUCTION

The study of fission of highly excited compound nuclei has emerged as a topic of great interest in recent years. The time scale of fission for highly excited heavy nuclei resulting from heavy ion induced fusion reactions has been extensively studied by measuring multiplicities of neutrons [1–3], charged particles [4,5] and giant dipole γ-rays [6–8]. These experimental results clearly reveal that there is excess emission of neutrons, charged particles and γ-quanta, in comparison with the standard statistical model predictions. This excess emission from the highly excited composite system is attributed to time delay or dynamical hindrance in the fission process. It, therefore, appears that the dissipative dynamical model would provide an appropriate description of nuclear fission at higher excitation energies. Very few measurements on evaporation residues (ERs) [9,10] have been carried out to understand the fission hindrance phenomenon. It is interesting to note that as a fused system moves from equilibrium position to saddle point and then saddle point to scission point, it keeps on emitting neutrons, protons, and gamma rays. Therefore, neutrons, charged particles and gamma ray multiplicities are not very sensitive to whether the emissions occur before or after the traversal of saddle point. On the other hand, ER measurement is a more sensitive method to understand the fission hindrance from equilibrium deformation point to saddle point because the evaporation probability from

*Electronic address: praveenshidling@yahoo.co.in

hot nuclei formed in heavy ion fusion reaction is sensitive to the dissipation strength inside the fission barrier. If there is any reduction in the fission width due to dissipation then there is a strong probability for survival of the compound nucleus. This is manifested in the evaporation residue cross section which is larger than predicted by the standard statistical model. The compound nucleus undergoing fission or surviving as an ER is decided mainly within the saddle point. Hence the measurement of ER formation probability provides the desired separation between pre-saddle and post-saddle dissipation. It is also pointed out by Frobrich *et al.* [11] that the ERs seem to be more sensitive probes for friction rather than neutrons, protons or γ-rays for studying the dynamics of fusion-fission process.

ERs de-excite to the ground state by the emission of gamma rays (nonstatistical in nature). These gamma rays carry valuable information on the spin distribution of ERs. Fission imposes the upper limit to the angular momentum carried by the evaporation residues from a heavy compound nucleus. If the fission branch is suppressed due to dissipation, then the spin population of ERs will be enhanced with the occurrence of the higher spin values. Thus spin distribution is also an additional parameter to study the dynamical competition between ERs and fission. The combined study of evaporation residues cross section and spin distribution gives a better understanding of fusion-fission dynamics than what is obtained by studying only the total evaporation residue cross section.

Here we report our measurements on total ER cross sections and spin distributions of ERs for a heavy compound nucleus (^{200}Pb*) over a range of excitation energies. Earlier, there was one such measurement but it was for lower fissility (^{194}Hg*) [10]. The present measurements have been performed over a range of energies around the Coulomb barrier where the dissipation effects are expected to be already set in for the fission [1,4,12], and the quasifission channels are absent [13].

The organization of the present paper is as follows. The experimental details and the results are presented in Sec. II. Section III reviews the basic ingredients of the model calculation and the data analysis, followed by summary and discussion in Sec. IV.

II. EXPERIMENTAL DETAILS AND RESULTS

The experiment was performed in two runs. In the first run, ^{16}O pulsed beam with the pulse separation of 4 μsec was taken from 15UD Pelletron accelerator at Inter University Accelerator Centre (IUAC), New Delhi. Evaporation residues (ERs) and spin distribution (gamma fold) measurements were carried out for ^{16}O + ^{184}W reaction in the energy range from $E_{\rm lab} = 84$ to 120 MeV. Enriched, isotopic ^{184}W target of thickness 210 μg/cm^2 on a 110 μg/cm^2 carbon backing was used. As the residues were of low energy (5.5 to 8 MeV), the carbon foil was made to face the beam to avoid energy loss of residues in carbon foil. The recoil mass spectrometer (Heavy Ion Reaction Analyzer), HIRA [14] was used for the identification of ERs. A set of BGO detectors was mounted at the target chamber for detecting gamma rays from ERs covering 48% of 4π solid angle. The PHOPDISC assembly [10], with the top and bottom flanges of the sliding seal target chamber modified in the form of reentrant bucket-like structure was used to accommodate the BGO detectors in a close geometry. 14 BGO detectors were used with seven detectors at the top and the remaining seven at the bottom. Elastically scattered oxygen ions were registered in two Si surface barrier detectors placed at $\pm 25^\circ$ with respect to the beam direction. A carbon foil of 40 μg/cm^2 thickness with large surface area was placed 10 cm downstream from the target to reset the charge state of ERs to statistical distribution. The HIRA spectrometer is 8.6 m long and its ion optics is based on electric-magnetic-electric dipole (ED-MD-ED) configuration with entrance and exit quadrupole doublets as shown in Fig. 1 (details can be found in Ref. [14]). HIRA was employed with full acceptance corresponding to a solid angle of 10 msr in order to transport the residues to the focal plane. ERs were detected at the focal plane by a large 50 $\times$ 50 mm^2 (active area) 2D position sensitive Si detector with a resistive layer at the front.

The measurements were performed at the laboratory beam energies of 84, 92, 100, 108, 116, and 120 MeV. We could go up to 120 MeV with a pulse separation of 4 μsec, beyond which the low intensity beam would not allow the locking of the terminal potential. Mass, recoil energy, and charge state scannings were done at each beam energy and, HIRA settings were optimized for most probable energy, mass, and charge state. The time taken by the ERs produced at the target chamber to reach the focal plane detector was 3.5 to 4 μsec. A pulsed beam, with a pulse separation of 4 μsec was used to record the time of flight (TOF) of slowly moving residues. The start signal for TOF was taken from focal plane Si detector and the stop signal was the RF used for pulsing, with 4 μsec pulse separation. The time of flight setup gave a clean separation of ERs from the beam like particles. Figure 2 shows the 2D plot of energy vs time of flight. We further recorded 14 TDC (time to

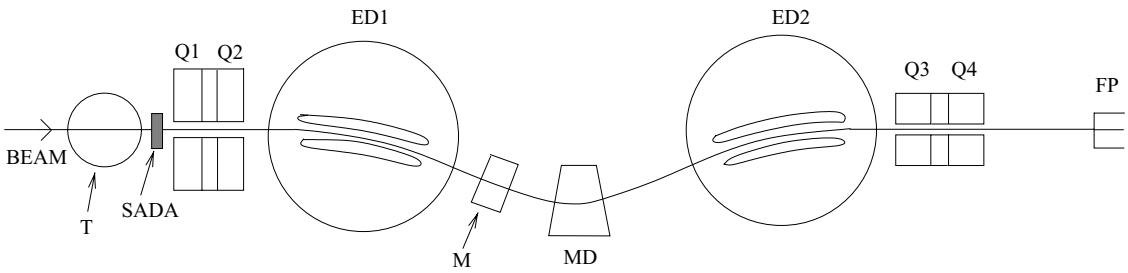

FIG. 1. Block diagram of Heavy Ion Reaction Analyzer (HIRA). Q1, Q2, Q3, Q4: Quadrupoles; ED1, ED2: Electric dipoles; MD: Magnetic dipole; M: Multipole; T: Target chamber; SADA: Solid Angle Defining Aperture; FP: Focal plane chamber.

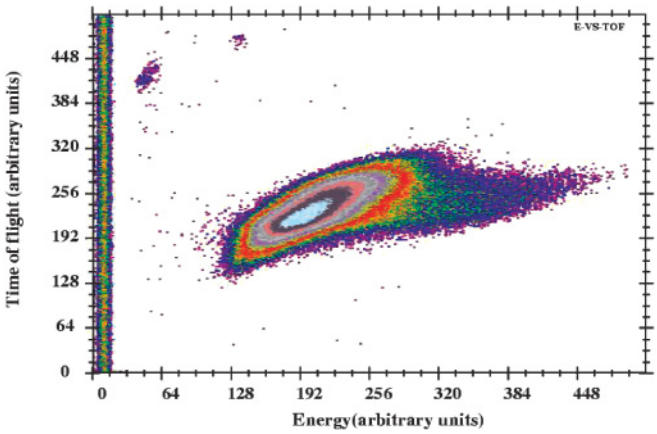

FIG. 2. (Color online) Two-dimensional plot of energy vs time of flight for the reaction ^{16}O+^{184}W at 100 MeV beam energy. The evaporation residues are at the center, while scattered beamlike particles (very few in numbers) are seen at the top-left corner of the plot, in two groups.

digital converter) spectra with ERs detected at the focal plane as the common start signal and timing from individual BGO detectors as the stop signal. These individual TDC spectra helped us to correct, in software, for background in each BGO signal while constructing the gamma fold distribution. In the second run, transmission efficiency of HIRA was determined experimentally for the chosen system.

A. Transmission efficiency of HIRA

The transmission efficiency of HIRA was determined by the gamma ray method at 100 MeV beam energy. A high resolution HPGe detector of 23% relative efficiency was mounted at the target chamber. The focal plane detector setup remained unchanged. Gamma rays were recorded by the HPGe detector in singles and in coincidence with ERs. The ratio of counts of a specific gamma line (corresponding to a particular ER) in coincidence spectrum ($N_{\rm coin}$) to that in the singles spectrum ($N_{\rm sing}$) gives the absolute transmission efficiency of HIRA for that ER:

$$\eta_{\rm HIRA} = \frac{N_{\rm coin}}{N_{\rm sing}}. \tag{1}$$

TABLE I. Transmission efficiencies for prominent ERs through HIRA (in percent) obtained by γ coincidence technique.

Residual nuclei	Gamma energy (keV)	$\eta_{\rm HIRA}$
^{194}Pb	581.8	$1.02 \pm 0.08\%$
^{195}Pb	969.1	$0.98 \pm 0.06\%$
^{195}Pb	739.1	$0.97 \pm 0.4\%$

Identified gamma lines from residual nuclei ^{194}Pb and ^{195}Pb and the calculated efficiencies are listed in Table I. Figure 3 shows the coincidence and singles spectra of gamma rays zoomed around the 581.82 keV (gamma line belonging to ^{194}Pb) peak.

B. Total evaporation residue cross section

The total evaporation residue cross section is obtained by using the relation

$$\sigma_{ER} = \frac{Y_{ER}}{C}\left(\frac{d\sigma}{d\Omega}\right)_R \Omega_M \frac{1}{\eta_{\rm HIRA}} \tag{2}$$

where Y_{ER} is the ER yield, C is monitor counts, Ω_M is the solid angle subtended by the surface barrier detector, $\eta_{\rm HIRA}$ is the transmission efficiency of HIRA, and $(d\sigma/d\Omega)_R$ is the differential Rutherford scattering cross section in the laboratory system. The evaporation residue cross sections deduced at different energies using Eq. (2) for the ^{16}O+^{184}W reaction are shown by solid circles in Fig. 4.

Total fusion cross sections (open triangles) are obtained by adding fission and evaporation residue cross sections. The fission cross sections have been taken from the literature [15].

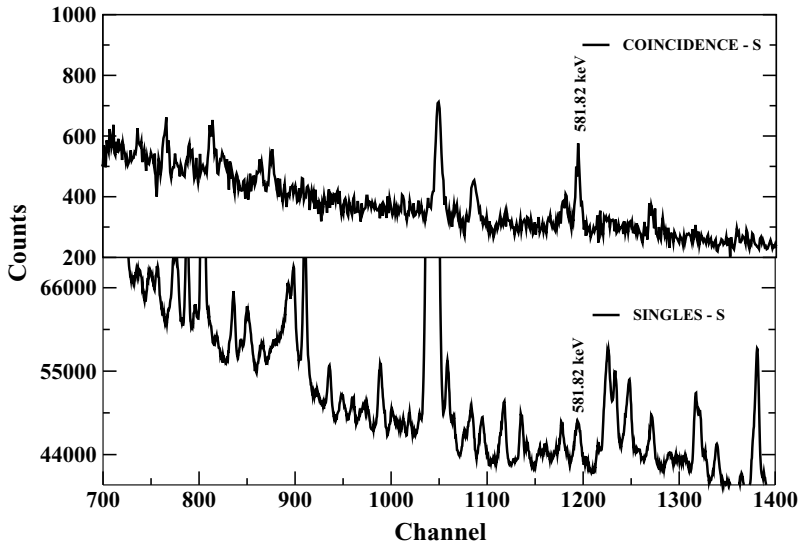

FIG. 3. γ-ray spectrum from the evaporation residues in the reaction ^{16}O+^{184}W at 100 MeV. Coincidence (top) and singles (bottom) spectra of gamma rays zoomed around the 581.82 keV.

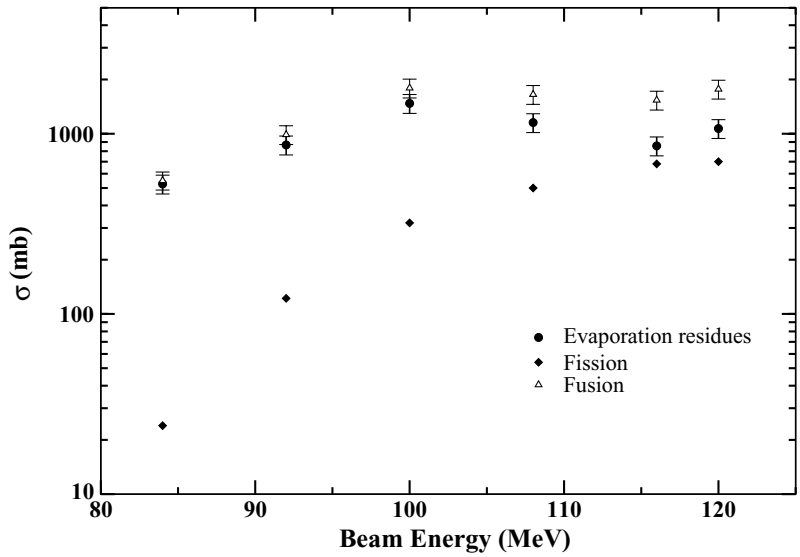

FIG. 4. Evaporation residue cross section for the reaction ^{16}O+^{184}W (solid points). Fission (data taken from Ref. [15]) and total fusion cross sections are shown by solid diamonds and open triangles, respectively.

C. Spin distribution of evaporation residues

The first step in this analysis was to extract the fold distribution from the TDC signals of BGO detectors. Fold distribution was generated from the software bit-pattern spectrum obtained using CANDLE software [16]. The generated fold distribution was in turn gated with ER events in the 2D spectrum of energy vs time of flight for further cleaning of the background. Figure 5 shows the gamma fold distribution for different beam energies.

Moments of the multiplicity distribution were extracted from the fold distribution by following the method explained in Ref. [17]. Some of the basic expressions used in the extraction of the moments are as follows. Let N be the number of identical detectors employed, each having a solid angle Ω, then the probability (P^M_{Np}) that a cascade of M uncorrelated γ-rays will cause number of p detectors to fire is given by

$$P^M_{N,p} = \binom{N}{p} \sum_{k=0}^{p} (-1)^{p-k} \binom{p}{k} [1-(N-k)\Omega]^M. \quad (3)$$

Let the probability of observing p-fold coincidence be denoted by $Q(p)$. Then its relation to γ-multiplicity probability distribution $P(M)$ is

$$Q(p) = \sum_{M=0}^{M_{\max}} P^M_{N,p}(\Omega) P(M). \quad (4)$$

This can be written in the form of factorial moments such as

$$Q(p) = \sum_{m=0}^{M} \left\langle \binom{M}{m} m! \right\rangle A_{p,m}(\Omega), \quad (5)$$

where

$$A_{p,m}(\Omega) = \frac{(-1)^m}{m!} \binom{N}{p} \sum_{k=0}^{p} (-1)^{p-k} \binom{p}{k} (N-k)^m \Omega^m. \quad (6)$$

By inverting Eq. (5), we obtain the factorial moments of the multiplicity distribution as

$$\left\langle \binom{M}{m} m! \right\rangle = \sum_{p=0}^{N} A^{-1}_{pm}(\Omega) Q(p). \quad (7)$$

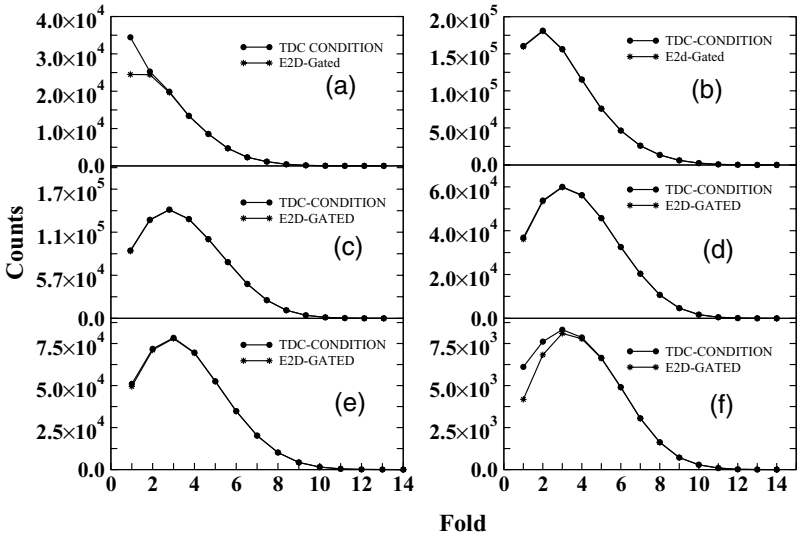

FIG. 5. Gamma fold distribution for the reaction ^{16}O+^{184}W at (a) 84 MeV, (b) 92 MeV, (c) 100 MeV, (d) 108 MeV, (e) 116 MeV, and (f) 120 MeV beam energies. Fold distributions are in turn gated with the ERs from 2D spectrum of energy vs time of flight for further cleaning of the background.

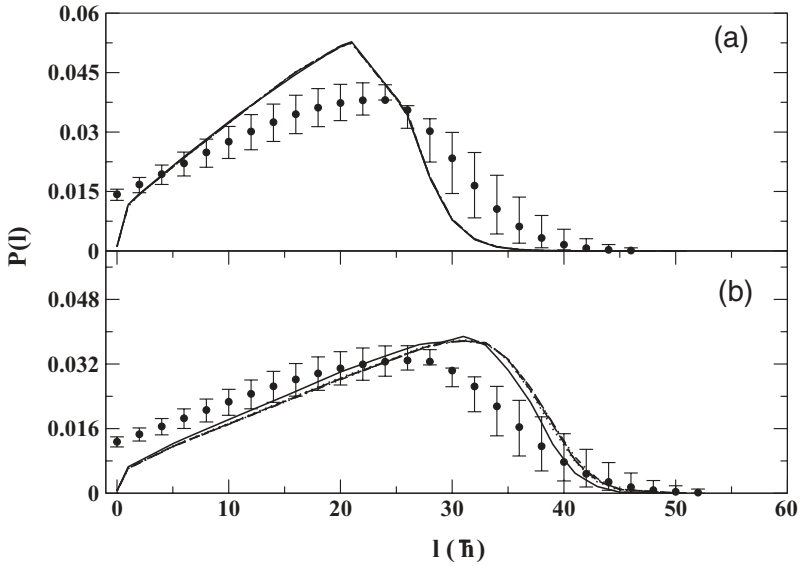

FIG. 6. Evaporation residue spin distributions for the reaction ^{16}O+^{184}W, at (a) 84 MeV and (b) 92 MeV beam energies are compared with statistical model calculation for $\gamma = 0$ (solid line), $\gamma = 2$ (dotted line), $\gamma = 3$ (dashed line), $\gamma = 4$ (dot long dash line), $\gamma = 5$ (double dot dash line).

A^{-1}_{pm} is the response matrix and is dependent on the detector solid angle and the number of detectors employed in the multiplicity setup. These factorial moments can be related in a straight forward way to different moments

$$\left\langle \binom{M}{m} m! \right\rangle = \langle M(M-1)\ldots\ldots(M-m+1)\rangle. \quad (8)$$

The multiplicity distribution was generated using the skewed gaussian multiplicity distribution of the form

$$Z(M) = \exp\left(-\frac{1}{2}\left(\frac{M-M_0}{\sigma_0(1+\epsilon\beta)}\right)^2\right), \quad (9)$$

where $\epsilon = \frac{M-M_0}{|M-M_0|}$; $M_0 = \langle M_\gamma \rangle$, σ_0 and β are the variance and the skewness parameters. Transformation of the multiplicity distribution to the spin distribution is made by assuming the ERs to be good rotors with two units of angular momentum carried away by each nonstatistical gamma ray [18]. Figures 6–8 show the plot of ER spin distribution for different beam energies. Since the zero fold probability cannot be extracted experimentally, spin distribution is nonzero at zero angular momentum. However, for looking at the effect of fission hindrance, higher l values are more important.

III. DATA ANALYSIS

We have compared the experimental evaporation residue cross sections and the spin distributions with the statistical model predictions for the decay of a compound nucleus. In the present calculation, the excited compound nucleus can emit neutrons and statistical giant dipole gammas before it undergoes fission. While the neutron and GDR gamma partial decay widths are obtained from the standard Weisskopf formula as given in Ref. [19], the partial fission widths are obtained from the Kramers modified Bohr-Wheeler formula [20] which incorporates the effect of nuclear dissipation on

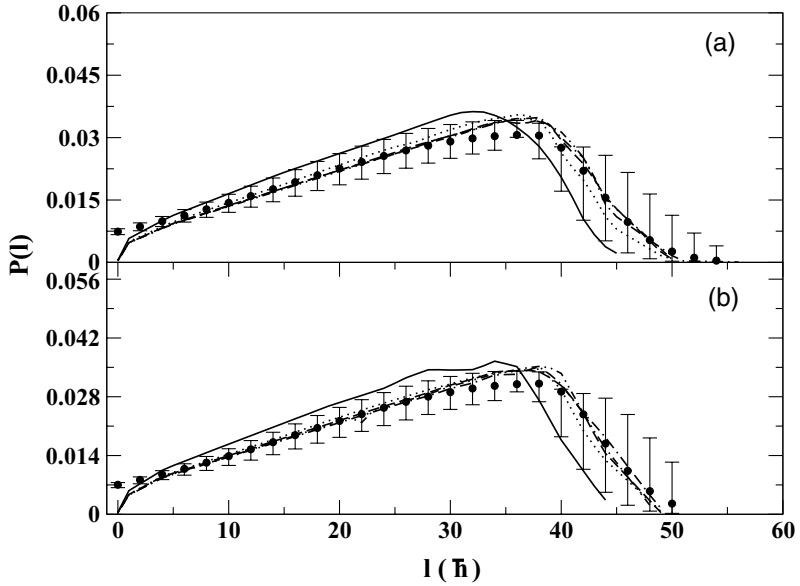

FIG. 7. Evaporation residue spin distributions for the reaction ^{16}O+^{184}W, at (a) 100 MeV and (b) 108 MeV beam energies are compared with statistical model calculations for $\gamma = 0$ (solid line), $\gamma = 2$ (dotted line), $\gamma = 3$ (dashed line), $\gamma = 4$ (dot long dash line), $\gamma = 5$ (double dot dash line).

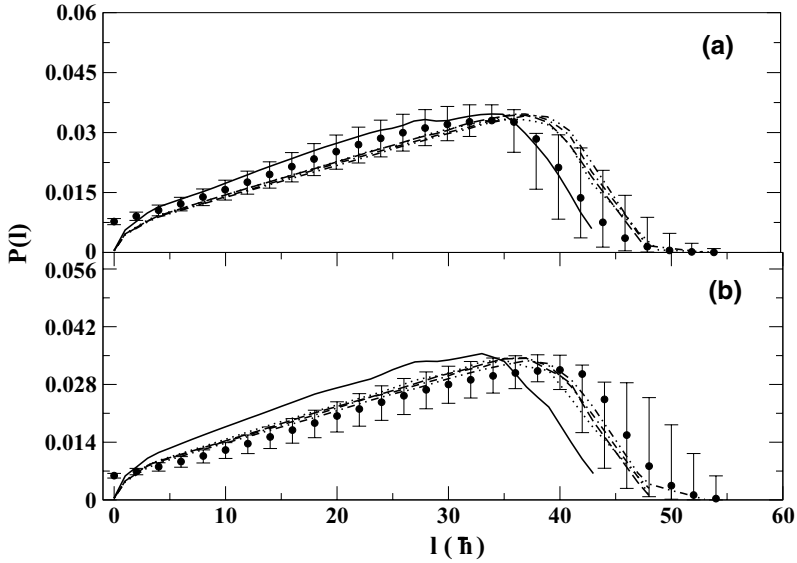

FIG. 8. Evaporation residue spin distributions for the reaction ^{16}O+^{184}W, at (a) 116 MeV and (b) 120 MeV beam energies are compared with statistical model calculations for $\gamma = 0$ (solid line), $\gamma = 2$ (dotted line), $\gamma = 3$ (dashed line), $\gamma = 4$ (dot long dash line), $\gamma = 5$ (double dot dash line).

fission and is given as

$$\Gamma_f^{\text{Kramers}} = \Gamma_f^{\text{BW}}[(1+\gamma^2)^{1/2} - \gamma], \tag{10}$$

where γ determines the strength of the dissipation and is treated as a free parameter here. The Bohr-Wheeler fission width is obtained using the fission barrier calculated from the finite range liquid drop model [21] for the nuclear potential. Using the above partial widths, the time evolution of the compound nucleus is followed in a statistical model code [22] till fission occurs or an evaporation residue is formed. The excitation energy and spin of the residual nucleus is recalculated after each emission of a neutron or a gamma.

We have assumed in the present calculation that the compound nucleus is formed by fusing the projectile fully with the target nucleus and processes such as fast fission or quasifission are not considered. The fusion cross section of the target and projectile in the entrance channel usually obeys the following spin distribution:

$$\frac{d\sigma(l)}{dl} = \frac{\pi}{k^2}\frac{(2l+1)}{1+\exp\left[\frac{(l-l_c)}{\delta l}\right]}, \tag{11}$$

where the values of the parameters l_c and δl are fixed by fitting the experimental fusion cross section. The total excitation energy of the compound nucleus is obtained from the beam energy of the projectile and the corresponding nuclear temperature by the relation $T = (E_{\text{int}}/a)^{1/2}$. The level density parameter is taken from the work of Ignatyuk *et al.* [23], which incorporates the nuclear shell structure effects at low excitation energies and goes smoothly to the liquid drop at a high excitation energy. An additional temperature dependence in the level density parameter is also introduced as outlined in Refs. [6,24]. The values of the level density parameter at equilibrium shape and at saddle configuration are used to calculate the neutron and fission widths, respectively.

In Fig. 9 we compare the experimental evaporation residue cross sections with the values predicted by the statistical

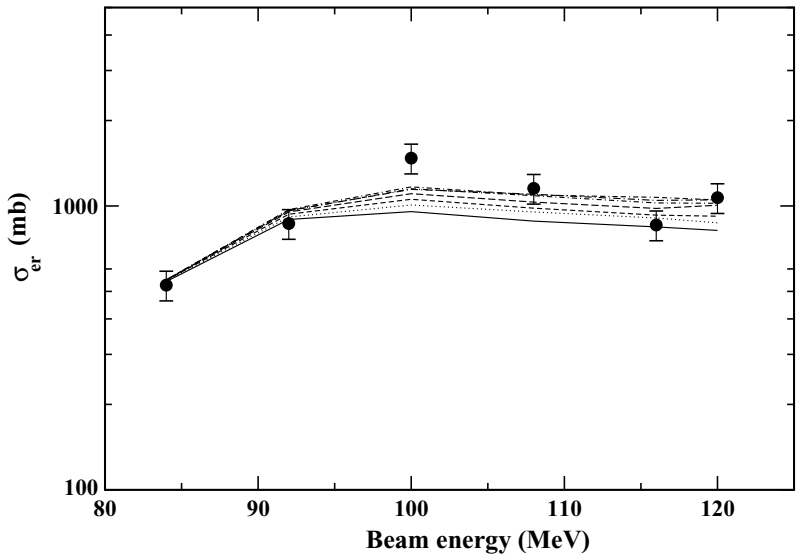

FIG. 9. Evaporation residue cross section (solid circles) with different excitation energies for the reaction ^{16}O+^{184}W are compared with the statistical model for $\gamma = 0$ (solid line), $\gamma = 0.5$ (dot line), $\gamma = 1$(dash line), $\gamma = 2$ (long dash line), $\gamma = 3$ (dot dash line), $\gamma = 4$ (dot long dash line), $\gamma = 5$ (dot double dash line).

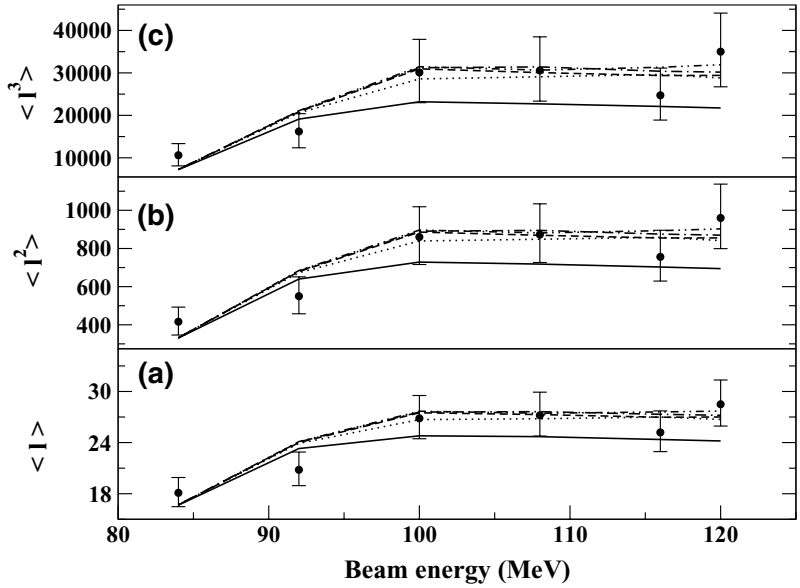

FIG. 10. Experimental mean (a), second (b), and third (c) moments of the evaporation residue spin distribution (solid circles) for the reaction ^{16}O+^{184}W at different beam energies are compared with statistical model calculations for $\gamma = 0$ (solid line), $\gamma = 2$ (dotted line), $\gamma = 3$ (dashed line), $\gamma = 4$ (dot long dash line), $\gamma = 5$ (double dot dash line).

model calculation. The solid line in Fig. 9 corresponds to the standard statistical model calculation, i.e., without the inclusion of nuclear dissipation ($\gamma = 0$). The standard statistical model calculation underestimates the evaporation residue cross section by about 20% especially in higher energy region. With the introduction of a dissipation into our calculation, the evaporation residue cross section increases with increase of the strength of dissipation though this increase is more pronounced at higher excitation energies of the compound nucleus. At lower excitation energies, where the fission cross section is a very small fraction of the fusion cross section, reduction of the fission cross section further by introducing a dissipation [Eq. (10)] hardly makes any noticeable change in the evaporation residue cross section. At higher excitation energies, where the fission cross section is a substantial part of the fusion cross section, the effect of slowing down of the fission process due to dissipation is clearly manifested as an increase of the evaporation residue cross section. We further note that the above increase saturates at $\gamma = 3$ and the evaporation residue cross section is not sensitive to higher values of γ. Our results therefore indicate that a dissipative force of strength $\gamma = 3$ in the fission dynamics of ^{200}Pb is essential to reproduce the systematic trend in the evaporation residue excitation function. Similar values of γ within the saddle point were also reported earlier from the analysis of GDR gamma ray multiplicity at higher excitation energies of ^{200}Pb [8] and also from evaporation residue cross section studies of ^{224}Th [24]. The present study provides evidence of a dissipative dynamics of fission even at somewhat lower excitation energies of ^{200}Pb. Before we conclude our discussion on evaporation residue cross section, we must draw attention to the fact that the experimental evaporation residue cross section at 100 MeV of beam energy is significantly higher than the theoretical prediction and that at 116 MeV of beam energy is slightly lower than the theoretical prediction with a value of $\gamma = 3$ (Fig. 9). In order to confirm these data we have repeated our measurements at 100 MeV in the second run and found that the value remains to be the same.

We shall next compare the calculated spin distribution of the evaporation residue with the experimental data. We first note in Fig. 6 that the calculated spin distribution are practically independent of the value of γ at lower excitation energies similar to the observation we made for the total evaporation residue cross sections. In Figs. 7 and 8 we find, however, that the standard statistical model ($\gamma = 0$) calculation underestimates the spin distributions at higher spin values compared to the experimental results. Calculations with higher values of γ shift the evaporation residue spin distributions to higher spin values and become closer to the experimental data. An overall agreement with the experimental data is attained for $\gamma = 3$ beyond which the distribution becomes insensitive to the value of γ, similar to our earlier observation regarding the total evaporation residue cross section. The standard statistical model ($\gamma = 0$) also underestimates the experimental mean, second and third moments of spin distribution which matches very well for the dissipation parameter $\gamma = 3$ as shown in Fig. 10.

IV. SUMMARY AND CONCLUSION

Summarizing, we have measured evaporation residue cross sections and its spin distributions for the ^{200}Pb compound nucleus formed in the collision of ^{16}O with ^{184}W nuclei at laboratory beam energies in the range of 84 to 120 MeV. The total fusion cross section is obtained by the sum of presently measured evaporation residue cross sections and the fission cross sections taken from the literature. Evaporation residue cross sections and the spin distributions for various energies have been compared with statistical model calculations.

The present study shows that the standard statistical model of fission (with no nuclear dissipation effects, i.e., $\gamma = 0$) cannot reproduce the systematic trend of evaporation residue cross sections and its spin distributions over the range of excitation energies considered here. Our analysis shows that a value of $\gamma = 3$ for the dissipation coefficient is required to

fit the evaporation residue cross section along with its spin distribution. The present study therefore provides evidence for some fission hindrance in ^{200}Pb in the measured energy region. It is further demonstrated in the present work that the evaporation residue spin distribution measurement provides another sensitive tool to investigate the fission hindrance in 200 mass region. It is therefore expected that more extensive measurements of evaporation residue cross sections along with spin distributions at higher excitation energies would lead to a better understanding of fission dynamics.

ACKNOWLEDGMENTS

The authors would like to thank the accelerator group of IUAC, New Delhi for providing an excellent pulsed beam of required rate during the experiment. Help received from target laboratory at IUAC, especially Mr. Abhilash, in making enriched ^{184}W target on C backing is acknowledged. One of the authors (P.D.S.) would like to thank IUAC for providing support through a UFUP Grant, and CSIR, New Delhi for financial support.

[1] D. J. Hinde, D. Hilscher, H. Rossner, B. Gebauer, M. Lehmann, and M. Wilpert, Phys. Rev. C **45**, 1229 (1992).
[2] J. O. Newton, D. J. Hinde, R. J. Charity, J. R. Leigh, J. J. M. Bokhorst, A. Chatterjee, G. S. Foote, and S. Ogaza Nucl. Phys. **A483**, 126 (1988).
[3] A. Saxena, A. Chatterjee, R. K. Choudhury, S. S. Kapoor, and D. M. Nadkarni, Phys. Rev. C. **49**, 932 (1994).
[4] J. P. Lestone, J. R. Leigh, J. O. Newton, D. J. Hinde, J. X. Wei, J. X. Chen, S. Elfstrom, and D. G. Popescu, Phys. Rev. Lett. **67**, 1078 (1991).
[5] H. Ikezoe, N. Shikazono, Y. Nagame, Y. Sugiyama, Y. Tomita, K. Ideno, I. Nishinaka, B. J. Qi, H. J. Kim, A. Iwamoto, and T. Ohtsuki Phys. Rev. C **46**, 1922 (1992).
[6] I. Diószegi, N. P. Shaw, I. Mazumdar, A. Hatzikoutelis, and P. Paul, Phys. Rev. C **61**, 024613 (2000).
[7] D. J. Hofman, B. B. Back, I. Diószegi, C. P. Montoya, S. Schadmand, R. Varma, and P. Paul, Phys. Rev. Lett. **72**, 470 (1994).
[8] I. Diószegi, N. P. Shaw, A. Bracco, F. Camera, S. Tettoni, M. Mattiuzzi, and P. Paul, Phys. Rev. C **63**, 014611 (2000).
[9] B. B. Back, D. J. Blumenthal, C. N. Davids, D. J. Henderson, R. Hermann, D. J. Hofman, C. L. Jiang, H. T. Penttilä, and A. H. Wuosmaa, Phys. Rev. C **60**, 044602 (1999).
[10] S. K. Hui, C. R. Bhuinya, A. K. Ganguly, N. Madhavan, J. J. Das, P. Sugathan, D. O. Kataria, S. Murlithar, Lagy T. Baby, Vandana Tripathi, Akhil Jhingan, A. K. Sinha, P. V. Madhusudhana Rao, N. V. S. V. Prasad, A. M. Vinodkumar, R. Singh, M. Thoennessen, and G. Gervais, Phys. Rev. C **62**, 054604 (2000).
[11] P. Frobrich and I. I. Gontchar, Nucl. Phys. **A563**, 326 (1993).
[12] M. Thoennessen and G. F. Bertsch, Phys. Rev. Lett. **71**, 4303 (1993).
[13] D. J. Hinde, J. R. Leigh, J. O. Newton, W. Galster, and S. Sie, Nucl. Phys. **A385**, 109 (1982).
[14] A. K. Sinha, N. Madhavan, J. J. Das, P. Sugathan, D. O. Kataria, A. P. Patro, and G. K. Mehta, Nucl. Instrum. Methods **339**, 543 (1994).
[15] J. S. Forster, I. V. Mitchell, J. U. Andersen, A. S. Jensen, E. Laegsgaard, W. M. Gibson, and K. Reichelt, Nucl. Phys. **A464**, 497 (1987).
[16] CANDLE software developed at Inter University Accelerator Centre (IUAC), New Delhi, India (Private Communication).
[17] S. Y. Vander Werf, Nucl. Instrum. Methods **153**, 221 (1978).
[18] M. L. Halbert, J. R. Benne, D. C. Hensley, K. Honkamen, T. M. Semkow, V. Abenante, D. G. Sarantites, and Z. Li, Phys. Rev. C **40**, 2558 (1989).
[19] P. Froebrich and I. I. Gontchar, Phys. Rep. **292**, 131 (1998).
[20] H. A. Kramers, Physica (Amsterdam) **7**, 284 (1940).
[21] A. J. Sierk, Phys. Rev. C **33**, 2039 (1986).
[22] G. Chaudhuri and S. Pal, Phys. Rev. C **65**, 054612 (2002).
[23] A. V. Ignatyuk, M. G. Itkis, V. N. Okolovich, G. N. Smirenkin, and A. Tishin, Yad. Fiz. **21**, 485 (1975) [Sov. J. Nucl. Phys. **21**, 255 (1975)].
[24] I. Diószegi, Phys. Rev. C **64**, 019801 (2001).